

# Assembly and Electrical Tests of the First Full-size Forward Module for the ATLAS ITk Strip Detector

C. García Argos<sup>a,\*</sup>, M. Hauser<sup>a</sup>, K. Jakobs<sup>a</sup>, K. Mahboubi<sup>a</sup>, U. Parzefall<sup>a</sup>,  
M. Wiehe<sup>a</sup>, L. Wiik-Fuchs<sup>a</sup>, B. Gallop<sup>g</sup>, A. Greenall<sup>e</sup>, P.W. Phillips<sup>g</sup>,  
C. Sawyer<sup>g</sup>, D. Sperlich<sup>b</sup>, M. Warren<sup>j</sup>, S.H. Abidi<sup>i</sup>, A.A. Affolder<sup>h</sup>,  
J. Bernabeu<sup>c</sup>, K. Dette<sup>i</sup>, Z. Dolezal<sup>f</sup>, V. Fadeyev<sup>h</sup>, P. Kodys<sup>f</sup>, C. Lacasta<sup>c</sup>,  
D. Madaffari<sup>c</sup>, R.S. Orr<sup>i</sup>, D. Rodriguez<sup>c</sup>, C. Solaz<sup>c</sup>, U. Soldevila<sup>c</sup>, R. Teuscher<sup>i</sup>,  
Y. Unno<sup>d</sup>, L. M. Velocce<sup>i</sup>

<sup>a</sup>Physikalisches Institut, Albert-Ludwigs-Universität Freiburg, Hermann-Herder-Str. 3,  
79104 Freiburg-im-Breisgau, Germany

<sup>b</sup>Institut für Physik, Humboldt-Universität zu Berlin, Newtonstraße, Berlin, Germany

<sup>c</sup>Instituto de Física Corpuscular (IFIC) - CSIC-University of Valencia, Parque Científico,  
C/Catedrático José Beltrán 2, E-46980 Paterna, Spain

<sup>d</sup>IPNS, KEK, 1-1 Oho, Tsukuba, Ibaraki 305-0801, Japan

<sup>e</sup>Particle Physics, University of Liverpool, Oliver Lodge Building, Department of Physics,  
Oxford Street, Liverpool, L69 7ZE, United Kingdom

<sup>f</sup>Faculty of Mathematics and Physics, Charles University, V Holesovickach 2, Prague,  
CZ18000 The Czech Republic

<sup>g</sup>Particle Physics Department, STFC Rutherford Appleton Laboratory, Chilton, Didcot,  
OX11 0QX, United Kingdom

<sup>h</sup>Santa Cruz Institute for Particle Physics (SCIPP), University of California, Santa Cruz,  
CA 95064, USA

<sup>i</sup>Department of Physics, University of Toronto, 60 Saint George St., Toronto M5S 1A7,  
Ontario, Canada

<sup>j</sup>Department of Physics and Astronomy, University College London, London, United  
Kingdom

## Abstract

The ATLAS experiment will replace the existing Inner Detector by an all-silicon detector named the Inner Tracker (ITk) for the High Luminosity LHC upgrades. In the outer region of the ITk is the strip detector, which consists of a four layer barrel and six discs to each side of the barrel, with silicon-strip modules as basic units. Each module is composed of a sensor and one or more flex circuits that hold the read-out electronics. In the experiment, the modules are mounted on support structures with integrated power and cooling. The modules are designed with geometries that accommodate the central (barrel) and forward (end-cap) regions, with rectangular sensors in the barrels and wedge shaped sensors in the end-caps. The strips lengths and pitch sizes vary according to the occupancy of the region.

In this contribution, we present the construction and results of the electrical tests of the first full-size module of the innermost forward region, named *Ring 0* in the ATLAS ITk strip detector nomenclature. This module uses a sensor with stereo annulus geometry, having four segments of strips of different lengths and pitch. The two innermost strips segments are read out through eight chips, for a total of 2048 strips, while the two outermost segments are read out through nine chips, for a total of 2304 strips. We introduce the assembly procedure that lead to the construction of the module as well as the testing during the intermediate

\*Corresponding author. e-mail: carlos.garcia.argos@physik.uni-freiburg.de  
Preprint submitted to Elsevier



steps.

---

## 39 1. Introduction

40 In the context of the High Luminosity LHC upgrade, the ATLAS tracker [1]  
41 will have to cope with much higher radiation and particle density, which forces  
42 changes in the whole tracker. The future Inner Tracker (ITk) will be an all-  
43 silicon detector, with a modular design that integrates cooling and electronics,  
44 and provides mechanical support [2].

45 Modules are the smallest unit of the detector, made from an n-in-p silicon  
46 strip sensor onto which read-out hybrids are glued and wire-bonded. The mod-  
47 ules are then glued onto the structures that integrate cooling, electronics and  
48 support. These are named *staves* in the barrel and *petals* in the end-caps. This  
49 contribution is centred on the latter, shown in Figure 1 [2].

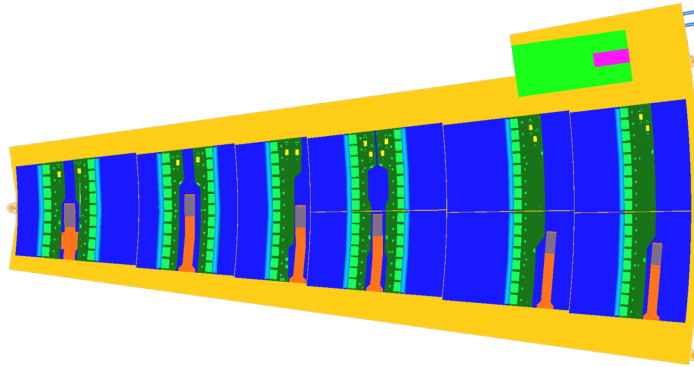


Fig. 1: Sketch of a *petal*, showing all six rings from left to right.

50 *Petals* are made of modules laid out in *Rings*, with the innermost ring named  
51 *Ring 0* (R0), increasing in number with radius for a total of six rings. The  
52 first module, using a full size sensor fabricated in a six-inch wafer, has been  
53 produced and tested. The sensors have a *stereo annulus* shape [3] and the read-  
54 out circuits, called hybrids, hold the read-out chips that are connected to the  
55 strips. The *Ring 0* sensor has four strips segments, with the two innermost  
56 comprising of 1024 read-out strips and the two outermost segments having 1152  
57 strips. The strip pitch varies along the length of the strips, between 73.5 and 84  
58 micrometres. The sensor is about 105 millimetres long and between 77 and 100  
59 millimetres wide. The sensor has an active thickness of about 300 micrometres.

60 The following sections describe the process used to build and test this first  
61 *Ring 0* module.

## 62 2. Hybrid Building

63 The read-out hybrids are flex circuit boards made in polyimide with multiple  
64 copper layers for the electrical connections. They hold dedicated read-out ASIC  
65 (Application Specific Integrated Circuit) chips, named ABC130 [4]. A Hybrid

66 Controller Chip, named HCC130 [2], is used to transmit the data from the  
67 ABC130 chips to outside the hybrid. Both chips are designed in a 130 nm  
68 CMOS process.

69 In the hybrid assembly process, the ASICs were glued onto the flex board us-  
70 ing ultra-violet cured glue for fast attachment, dispensed with a programmable  
71 robot. Special tooling is used for precise positioning of the chips on the boards,  
72 as well as for control of the glue thickness. The chips were held by vacuum  
73 on the pick-up tools and the hybrid flex circuits were held by vacuum on a  
74 custom built and precisely machined jig. The curing of the glue was done by  
75 illuminating with an ultra-violet LED for 120 seconds.

76 After the chips were attached onto the board, the electrical connections of  
77 the chips to the hybrid PCB were performed by automated wire-bonding.

78 Once assembled and wire-bonded, the hybrids were electrically tested, to  
79 verify the functionality of all the read-out chips by reading out their registers  
80 and measuring the voltages on the hybrids and at the chips linear regulators.  
81 Their analogue performance was also assessed in further electrical tests. Noise  
82 measurements and calibrations were run to assess the performance of the chips,  
83 and the values were compared before and after assembly of the full module. De-  
84 tails about the tests performed on the constructed hybrids and module presented  
85 in this paper are given in Section 4.2.

### 86 3. Module Building

87 The tested hybrids were glued on the sensor using an epoxy glue that is cured  
88 for at least ten hours at room temperature. The sensor was held by vacuum on  
89 another custom built precision jig. The same tools used to glue the ASICs were  
90 used to pick-up the hybrids and hold them during the glue curing process.

91 After the glue was fully cured, the sensor electrical characteristics were mea-  
92 sured on the probe station again, prior to wire-bonding of all the strips to the  
93 front-end channels of the chips. The measurements performed on the sensor are  
94 presented in Section 4.1.

95 Figure 2 shows a picture of the assembled module. The front-end channels  
96 were bonded using four rows of bonds with different lengths and loop heights.  
97 The use of four rows poses extra difficulty when assessing the correctness of the  
98 bonding process. No bonds failed in this four row bonding and there were no  
99 short circuits between bonds.

100 In a final step, a power-board was glued onto the sensor and connected to the  
101 hybrids. This power-board includes a DC-DC converter [5] which steps down  
102 an input voltage between 6 and 12 V to 1.5 V. By using DC-DC conversion, the  
103 power losses on the cables are reduced, resulting in a reduction of the material  
104 inside the tracker and a more stable operation.

### 105 4. Electrical Tests

#### 106 4.1. Sensor Testing

107 The sensors used for module building are measured during the whole assem-  
108 bly process. Current and capacitance as a function of the bias voltage (I/V and  
109 C/V) of the bare sensor are measured on a probe station. The depletion voltage  
110 is extracted from the C/V curve and is found to be at around 300 V [6].

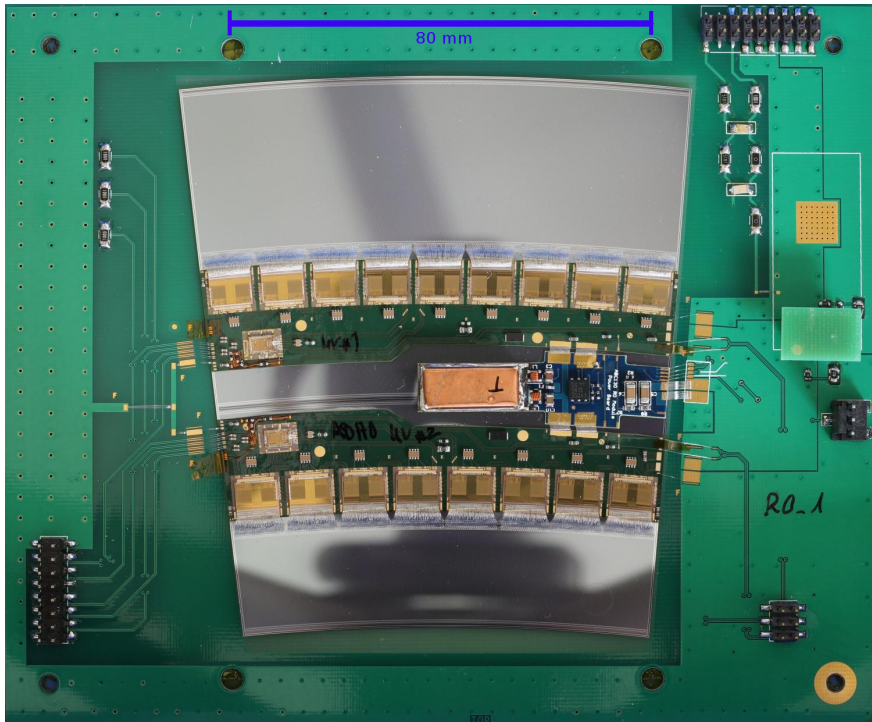


Fig. 2: The first completely assembled R0 module on a test-frame, showing the sensor, both hybrids and the power-board. The bottom hybrid is called ROH0 and the top hybrid is called ROH1.

111 After the hybrid has been glued onto the sensor, another I/V curve is taken  
 112 in order to check for sensor degradation due to the gluing process.

113 Last, a final I/V is taken after all the strips are wire-bonded to the read-  
 114 out front-end channels on the ASICs. Figure 3 shows the results of the I/V  
 115 curves taken. It exhibits a slight worsening of the behaviour after gluing and  
 116 wire-bonding, which points at possible signs of mechanical stress on the sensor.

#### 117 4.2. Module Testing

118 Digital and analogue tests were performed on the fully assembled module.  
 119 The digital tests involve communicating with the read-out chips and configuring  
 120 them.

121 For all tests, the module is powered in two ways: with a direct connection  
 122 to the power supply which has to provide 1.5 V to the hybrids, or with a power-  
 123 board, fed with 11 V from the power supply.

124 The analogue tests performed on the fully assembled module include the  
 125 following:

- 126 • *Strobe Delay*, consisting of varying the phase of the charge injection rela-  
 127 tive to the trigger signal to the chips. This test is used to find the timing  
 128 at which all injected pulses are detected at low thresholds, and is essential  
 129 for the following two tests to work properly.

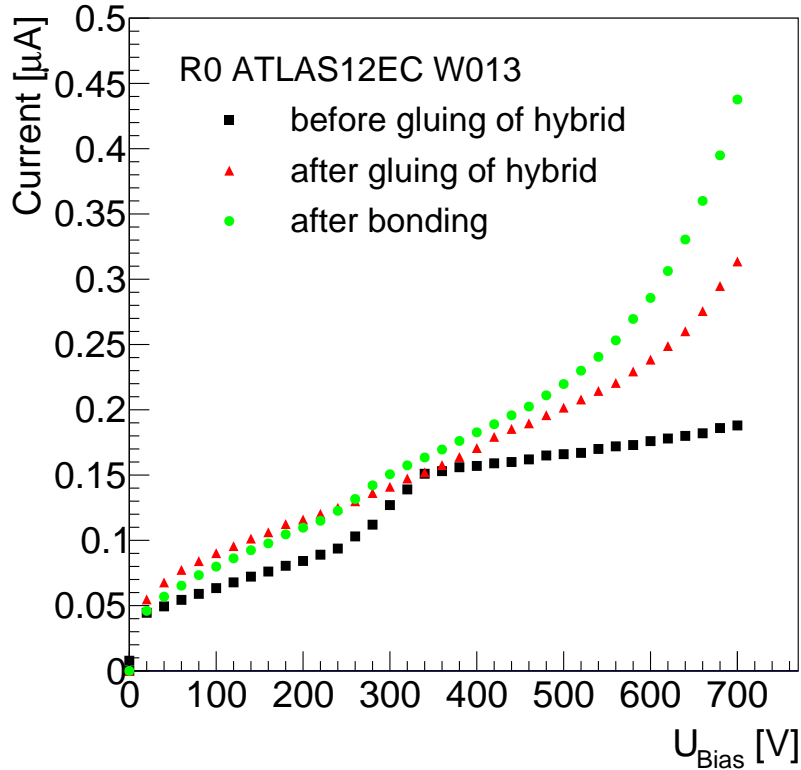


Fig. 3: I/V curves of the sensor used for the first R0 module during the whole building process: before and after gluing, and after wire-bonding. All measurements were performed on the same probe station.

- 130 • *Trim Range*, in which the trims in the chips are optimised in order to  
131 minimise the variations in the response among channels. It consists of  
132 a series of threshold scans with a fixed injected charge, varying the trim  
133 settings of the chips, in order to find the ones that result in a homogeneous  
134 response. The result of this test is either a failure due to untrimmable  
135 channels or chips, or the trim settings for each channel.
- 136 • *Response Curve*, which consists of ten threshold scans with varying in-  
137 jected charges. The output noise of the front-end is extracted from the  
138 variance of the occupancy for each value of injected charge, and the me-  
139 dian point, or  $V_{t50}$ , is extracted and used to determine the gain in mV/fC  
140 from an exponential fit with all ten points. Using the gain and the output  
141 noise, the input noise is calculated in electrons Equivalent Noise Charge  
142 ( $e^-ENC$ ).
- 143 • *Noise Occupancy*, a high statistics threshold scan is performed without  
144 injected charge, in order to determine the noise occupancy of each channel  
145 as a function of the threshold.

146 The *Response Curve* test was performed at different sensor bias voltages,

147 scanning from under-depletion up to over-depletion of the bulk. Figure 4 shows  
 148 the results for this bias voltage scan, exhibiting the expected behaviour of noise  
 149 reduction until the sensor is fully depleted.

150 It also shows the noise values of each strip segment, which are different due  
 151 to the varying lengths of the segments: 19, 24, 29 and 32 millimetres. Noise  
 152 is dependent on other parameters, such as temperature, front-end tuning and  
 153 total capacitance. The capacitance is dependent on the strip length as well as  
 154 other added capacitance such as a metallic plane over the sensor. The areas  
 155 where a hybrid is glued onto the sensor have an extra capacitance, which drives  
 156 the noise up, and this is observed for the second and third segments. These  
 157 results correspond to the module prior to the attachment of the power-board.

158 The comparison between the bare hybrids and the fully assembled module  
 159 without power board shows a noise increase of around 180 electrons for the first  
 160 (shortest) strip segment, 272 for the second segment, 350 for the third segment,  
 161 and 354 for the fourth (longest) segment. As mentioned above, the segments  
 162 for which there is a hybrid glued onto the sensor, exhibit a larger noise increase  
 163 due to the extra capacitance. This results in the third segment having a noise  
 164 increase close to the fourth segment, despite the difference in strip length.

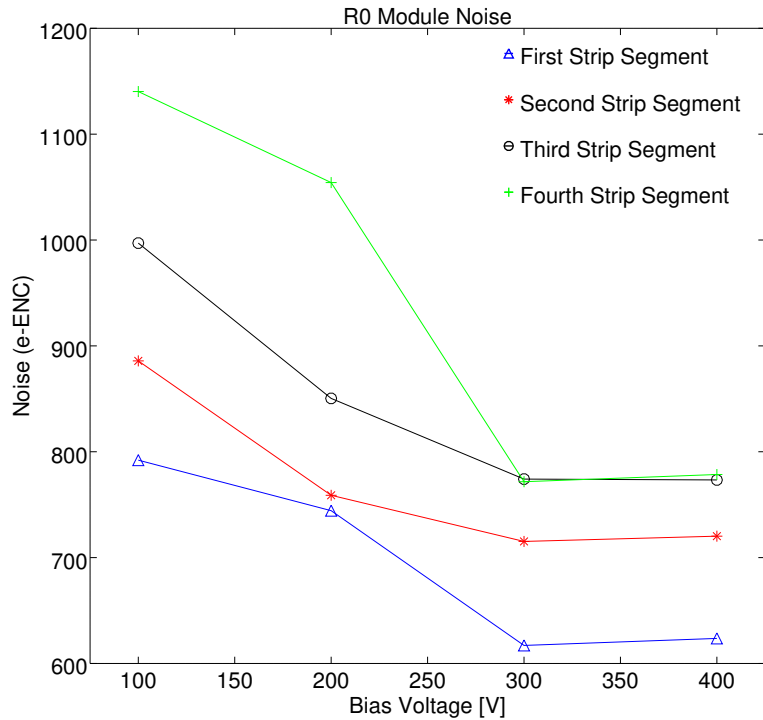


Fig. 4: Input noise for different bias voltages.

165 The noise was measured before and after attaching and connecting the  
 166 power-board. Figure 5 shows the comparison of the noise before and after  
 167 attaching the power-board on the module. As shown in Figure 6, only the four

168 chips on the right of R0H0 and the strips running underneath the power-board,  
169 corresponding to the second strip segment, are shown in this plot. *Chip 16* is  
170 the first chip from the right and *Chip 19* is the fourth. Chip to chip variations  
171 in the noise without the power-board are due to gain differences amongst chips,  
172 which are caused by the front-end tuning.

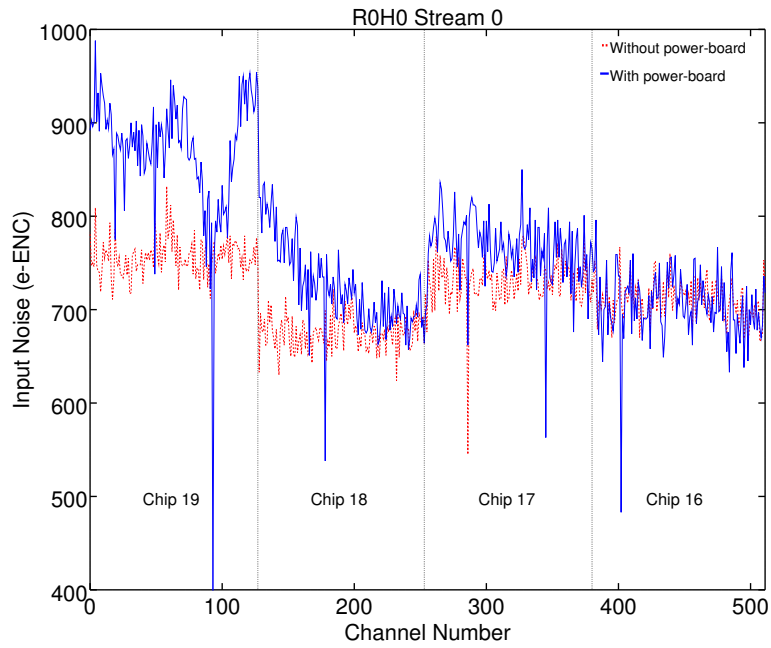


Fig. 5: Input noise measurements with (solid red line) and without (dashed blue line) the power-board, for the four rightmost chips of the R0H0 hybrid, strips underneath the power-board.

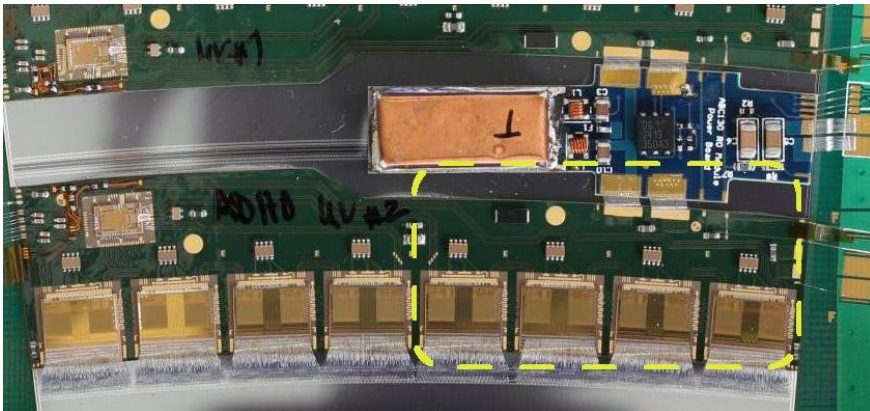


Fig. 6: Area of the module exhibiting the noise increase due to the power-board.

173 This extra noise is associated with a leakage of the magnetic field in the  
174 inductance used to store the energy for the DC-DC conversion. This noise  
175 excess can be addressed by improving the shielding of the coil.

176 Even with this additional noise, the module fulfils the requirement of less  
177 than 1000 electrons which would result in a signal to noise ratio larger than 10  
178 after irradiation at the full HL-LHC fluence [2].

179 For the noise occupancy tests, results show values well below the requirement  
180 of less than  $10^{-3}$  channel noise occupancy at a threshold that results in detection  
181 efficiency greater than 99%.

## 182 5. Conclusions

183 The first full-size module using a *stereo annulus* shape sensor, fabricated  
184 in a six-inch wafer for the ATLAS ITk Strips Upgrade has been successfully  
185 built and tested. This module is one of the components of the forward region,  
186 covering the innermost ring.

187 This contribution shows that the building process is under control, with  
188 precision attachment of the read-out chips, gluing of the hybrids onto the sensor  
189 and the wire-bonding step.

190 All performance parameters extracted from the electrical tests are consistent  
191 with the sensor characteristics and comply with the specified values for the  
192 upgrade of the ATLAS tracker.

193 The addition of the power-board is still under study, with a slight noise  
194 increase due to leakage of the magnetic field generated by the coil that is part  
195 of the DC-DC converter.

## 196 6. Acknowledgements

197 The research was supported and financed in part by Canada Foundation for  
198 Innovation, the National Science and Engineering Research Council (NSERC)  
199 of Canada under the Research and Technology Instrumentation (RTI) grant  
200 SAPEQ-2016-00015; the Federal Ministry of Education and Research, BMBF,  
201 Germany; the UK's Science and Technology Facilities Council; and USA De-  
202 partment of Energy, Grant DE-SC0010107.

## 203 References

- 204 [1] ATLAS Collaboration, *The ATLAS Experiment at the CERN Large Hadron*  
205 *Collider*, JINST 3 (2008) S08003.
- 206 [2] ATLAS Collaboration, *Technical Design Report for the ATLAS Inner*  
207 *Tracker Strip Detector*, CERN-LHCC-2017-005. April 2017.
- 208 [3] C. Lacasta et al., *Design of the first full size ATLAS ITk Strip sensor for*  
209 *the endcap region*, HSTD11&SOIPIX. December 2017.
- 210 [4] J. Kaplon and M. Noy, *Front end electronics for SLHC semiconductor track-*  
211 *ers in CMOS 90 nm and 130-nm processes*, IEEE Trans.Nucl.Sci. 59 (2012)  
212 1611–1620.



- 213 [5] F. Faccio et al., *FEAST2: A Radiation and Magnetic Field Tolerant Point-*  
214 *of-Load Buck DC/DC Converter*, 2014 IEEE Radiation Effects Data Work-  
215 shop (REDW).
- 216 [6] R. Hunter et al., *First bulk and surface results for the ATLAS ITk Strip*  
217 *stereo annulus sensors*, HSTD11&SOIPIX. December 2017.